Monthly Notices
of the
ROYAL ASTRONOMICAL SOCIETY

MNRAS **476,** 399–406 (2018) doi:10.1093/mnras/sty210

Revealing two radio-active galactic nuclei extremely near PSR J0437−4715

Zhixuan Li,[1,2,3] Jun Yang,[1,4,5★] Tao An,[5,6★] Zsolt Paragi,[7] Adam Deller,[8] Cormac Reynolds,[9] Xiaoyu Hong,[5,6] Jiancheng Wang,[1,3] Hao Ding,[2,5,6] Bo Xia,[5,6] Zhen Yan[5,6] and Li Guo[5,6]

[1] *Yunnan Observatories, Chinese Academy of Sciences, 650216 Kunming, Yunnan, China*
[2] *University of Chinese Academy of Sciences, 19A Yuquan Road, Shijingshan District, 100049 Beijing, China*
[3] *Key Laboratory for the Structure and Evolution of Celestial Objects, Chinese Academy of Sciences, 650216 Kunming, China*
[4] *Department of Space, Earth and Environment, Chalmers University of Technology, Onsala Space Observatory, SE-439 92 Onsala, Sweden*
[5] *Shanghai Astronomical Observatory, Chinese Academy of Sciences, 200030 Shanghai, China*
[6] *Key Laboratory of Radio Astronomy, Chinese Academy of Sciences, 210009 Nanjing, China*
[7] *Joint Institute for VLBI ERIC (JIVE), Postbus 2, NL-7990 AA Dwingeloo, the Netherlands*
[8] *Centre for Astrophysics, and Supercomputing, Swinburne University of Technology, John St, Hawthorn, VIC 3122, Australia*
[9] *CSIRO Astronomy and Space Science, Kensington, WA 6151, Australia*

Accepted 2018 January 20. Received 2018 January 19; in original form 2017 October 16

ABSTRACT

Newton's gravitational constant G may vary with time at an extremely low level. The time variability of G will affect the orbital motion of a millisecond pulsar in a binary system and cause a tiny difference between the orbital period-dependent measurement of the kinematic distance and the direct measurement of the annual parallax distance. PSR J0437−4715 is the nearest millisecond pulsar and the brightest at radio wavelengths. To explore the feasibility of achieving a parallax distance accuracy of one light-year, comparable to the recent timing result, with the technique of differential astrometry, we searched for compact radio sources quite close to PSR J0437−4715. Using existing data from the Very Large Array and the Australia Telescope Compact Array, we detected two sources with flat spectra, relatively stable flux densities of 0.9 and 1.0 mJy at 8.4 GHz and separations of 13 and 45 arcsec. With a network consisting of the Long Baseline Array and the Kunming 40-m radio telescope, we found that both sources have a point-like structure and a brightness temperature of $\geq 10^7$ K. According to these radio inputs and the absence of counterparts in other bands, we argue that they are most likely the compact radio cores of extragalactic active galactic nuclei, rather than Galactic radio stars. The finding of these two radio active galactic nuclei will enable us to achieve a sub-pc distance accuracy with in-beam phase-referencing very-long-baseline interferometric observations and provide one of the most stringent constraints on the time variability of G in the near future.

Key words: astrometry – pulsars: individual: PSR J0437−4715 – galaxies: jets.

1 INTRODUCTION

Millisecond pulsars (MSPs) are neutron stars that have been 'recycled' via accretion of material from a companion (Alpar et al. 1982) and spin with a period usually shorter than about 10 ms. Compared with those normal pulsars that spin more slowly, MSPs have much more stable rotation. Thus, their radio pulses can be used as extremely accurate clocks for the study of relativistic gravitation (e.g. Manchester 2015).

PSR J0437−4715 is an MSP discovered by Johnston et al. (1993) with the 64-m Parkes radio telescope in Australia. PSR J0437−4715 is the nearest MSP and the brightest in the radio band. It has a statistical mean flux density of 150 mJy at 1.4 GHz (e.g. Dai et al. 2015). As one of the most stable and precisely timed pulsars, it is a cornerstone of efforts to use a pulsar timing array to search for nanoHertz-frequency gravitational waves (e.g. Shannon et al. 2015) and has been observed intensively with the Parkes telescope for more than 20 yr. Its timing model has been improved continuously

★ E-mail: jun.yang@chalmers.se (JY); antao@shao.ac.cn (TA)

Table 1. Summary of the radio observations of the PSR J0437−4715 field.

Project code	Array	N_{ant}	Date	Freq. (GHz)	Bw (MHz)	Time (min)	Beam FWHM	Sensitivity (mJy beam^{-1})
AH0595	VLA	12	1996 Oct 12	1.435	100	76	5.″40 × 0.″79 at −0.°22	0.11
AH0595	VLA	15	1996 Oct 12	4.860	100	100	6.″40 × 0.″95 at +0.°30	0.05
V190A	ATCA	6	2006 May 13	8.428	40	596	2.″28 × 1.″36 at −0.°47	0.10
V190E	ATCA	5	2006 Nov 16	8.428	40	688	6.″05 × 4.″03 at −2.°74	0.18
V190G	ATCA	5	2007 Mar 22	8.428	40	694	10.″90 × 7.″39 at +0.°41	0.13
V190K	ATCA	6	2007 Nov 12.	8.428	40	697	2.″09 × 1.″44 at −0.°22	0.09
V190M	ATCA	6	2009 Dec 12	8.457	384	579	2.″33 × 1.″35 at −5.°86	0.14
V190O	ATCA	5	2010 Oct 27	8.424	50	609	27.″1 × 20.″4 at −81.°70	0.13
V539	LBA+KM	5	2015 Nov 18	2.285	32	208	0.″015 × 0.″0056 at +41.°3	0.09

Note. Columns give (1) project code, (2) array name, (3) total number of telescopes (N_{ant}), (4) observation date, (5) observation frequency in GHz, (6) total bandwidth in MHz, (7) total on-source time in min, (8) beam full width at half-maximum (FWHM) and (9) image sensitivity in mJy beam^{-1}.

by timing analyses (e.g. Verbiest et al. 2008). By using longer time baseline data and modelling non-stationary noise, Reardon et al. (2016) significantly improved the timing measurements of the proper motion μ, orbital period P_b and orbital period derivative $\dot{P}_b$. The observed orbital period derivative is dominated by a 'kinematic' term due to the transverse motion of the pulsar; accordingly, the timing observables can be used to obtain a kinematic distance of $D_k = (c/\mu^2)(\dot{P}_b/P_b) = 156.79 \pm 0.25$ pc. To date, this is the most precise distance measurement to a radio pulsar.

The distance to a radio pulsar can also be measured accurately with multi-epoch very-long-baseline interferometric (VLBI) observations of the annual parallax π. The position measurements are made with respect to a nearby extragalactic source, the position of which is assumed to be stationary, i.e. a phase-referencing calibrator. Differential VLBI astrometry performed on PSR J0437−4715 can provide not only an accurate parallax distance D_π but also a stringent constraint on the stability of Newton's gravitational constant G, i.e. $\dot{G}$. This is because the difference between D_π and D_k represents the maximum contribution from the potential $\dot{G}$. Deller et al. (2008) measured $D_\pi = (1/\pi) = 156.3 \pm 1.3$ pc ($\pi = 6396 \pm 54$ microarcsec (μas)) for PSR J0437−4715 with Australia Long-Baseline Array (LBA) astrometry at 8.4 GHz and estimated a tight upper limit of $\dot{G}/G = (-5 \pm 26) \times 10^{-13}$ yr^{-1}, together with an earlier measurement of $D_k = 157.0 \pm 2.4$ pc (Verbiest et al. 2008). Because D_k has recently been measured with unprecedented precision, 0.25 pc (Reardon et al. 2016), it is becoming a key question in the study of $\dot{G}$ as to whether it is also feasible to gain a much more accurate D_π in the near future.

The easiest and most reliable way to improve the VLBI parallax accuracy is to use a phase-referencing source as close to the target source as possible (e.g. the PSRπ project: Deller et al. 2016). The small angular separation means that differential propagation effects through the ionosphere and troposphere are minimized and moreover ensures that all radio telescopes can observe both sources simultaneously. Thus, systematic phase errors affecting the target can be calibrated and removed very accurately via solutions obtained from the phase-referencing source. Based on the in-beam phase-referencing technique, a parallax accuracy of ∼15 μas was achieved by Deller et al. (2013) for PSR J2222−0137. According to the known pulsar parallax measurements, the best attainable parallax accuracy has an empirical dependence of about 1–2 μas per arcmin on the calibrator-target separation (Chatterjee et al. 2004; Deller et al. 2013; Kirsten et al. 2015). However, this 'floor' is the best attainable result of a perfect calibrator: one that is bright enough to enable calibration solutions for short integration time and does not exhibit any significant source structure variations.

This article is organized in the following sequence. Section 2 describes the radio experiments we used and the data reduction steps we followed. Section 3 reports the imaging and data analysis results. Section 4 discusses the identification of two radio sources that we detected in the radio observations, the feasibility of achieving a sub-pc parallax precision for PSR J0437−4715 with in-beam phase-referencing VLBI observations and the implications of a more stringent constraint on $\dot{G}$. Section 5 gives the final conclusions.

2 OBSERVATIONS AND DATA REDUCTION

To search for extragalactic compact radio sources quite close to PSR J0437−4715, we re-analysed an early Very Large Array (VLA) experiment (project code: AH0595) provided by the NRAO Science Data Archive.[1] After finding two candidates within a one-arcmin circle from PSR J0437−4715, we performed in-beam phase-referencing VLBI observations of them with the Australia Long-Baseline Array (LBA) plus the Chinese Kunming 40-m radio telescope at 2.3 GHz (project code: V539). Both the VLA data and the VLBI data were calibrated in AIPS (Astronomical Image Processing System: Greisen 2003). The iterative loop of source deconvolution and self-calibration was conducted in DIFMAP (Shepherd, Pearson & Taylor 1994). To study their flux density stability, we also reduced the existing interferometric data (project code: V190), which comprised a multi-epoch series spanning about 4.5 yr and as observed by the Australia Telescope Compact Array (ATCA) at 8.4 GHz during the LBA observations of PSR J0437−4715 (Deller et al. 2008). The ATCA data were calibrated in the software package MIRIAD (Sault, Teuber & Wright 1995).

The observational information about these experiments and the final intensity image parameters are listed in Table 1. The total flux densities of PSR J0437−4715 and the two faint sources, named R1 and R2, and their observation dates and frequencies are reported in Table 2.

2.1 VLA data at 1.4 and 5 GHz

The VLA experiment is one of the deepest observations of PSR J0437−4715. It was performed in the array configuration of A

[1] https://archive.nrao.edu/archive/advquery.jsp

Table 2. Summary of the total flux-density measurements.

Name	MJD	Flux (mJy)	Frequency (GHz)
J0437−4715	50369.4	166.81 ± 0.11	1.435
R1	50369.4	0.97 ± 0.11	1.435
R2	50369.4	0.77 ± 0.11	1.435
J0437−4715	50369.4	14.90 ± 0.05	4.860
R1	50369.4	1.35 ± 0.05	4.860
R2	50369.4	1.67 ± 0.05	4.860
J0437−4715	53869.1	4.04 ± 0.10	8.428
R1	53869.1	1.06 ± 0.10	8.428
R2	53869.1	0.99 ± 0.10	8.428
J0437−4715	54055.6	4.01 ± 0.18	8.428
R1	54055.6	0.83 ± 0.18	8.428
R2	54055.6	0.88 ± 0.18	8.428
J0437−4715	54181.3	4.01 ± 0.13	8.428
R1	54181.3	0.90 ± 0.13	8.428
R2	54181.3	1.09 ± 0.13	8.428
J0437−4715	54416.6	3.75 ± 0.09	8.428
R1	54416.6	0.88 ± 0.09	8.428
R2	54416.6	1.01 ± 0.09	8.428
J0437−4715	55177.5	4.01 ± 0.15	8.457
R1	55177.5	1.10 ± 0.15	8.457
R2	55177.5	1.00 ± 0.15	8.457
J0437−4715	55496.7	4.44 ± 0.13	8.424
R1	55496.7	0.79 ± 0.13	8.424
R2	55496.7	1.23 ± 0.13	8.424
J0437−4715	57344.6	60.32 ± 0.15	2.285
R1	57344.6	0.83 ± 0.09	2.285
R2	57344.6	0.66 ± 0.09	2.285

and D on 1996 October 12. The whole array was divided into two sub-arrays to observe PSR J0437−4715 simultaneously at both 1.4 and 5 GHz. Because of the quite low declination of PSR J0437−4715, both sub-arrays had relatively high resolution (up to sub-arcsec) in the east–west direction only. The source J0440−4333 (B0440−435) was observed as the phase-referencing calibrator. The multi-frequency monitoring observations performed by Tingay et al. (2003) with the ATCA between 1996 October and 2000 February show that J0440−4333 was quite stable, with a variability index of 0.02 at 1.38 GHz and 0.10 at 4.80 GHz. We also used J0440−4333 as the flux density calibrator in the subsequent data reduction, given its known ATCA mean flux-density measurements of 4.53 Jy at 1.38 GHz and 3.19 Jy at 4.80 GHz. According to the ATCA monitoring results, we took ∼2 per cent as the 1σ systematic flux density error in both bands. Following the standard VLA data reduction recipe in the AIPS cookbook,[2] we removed some bad data at the beginning of each scan, set the flux density of J0440−4333, ran both self-calibration and bandpass calibration on the calibrator and applied all solutions to both the calibrator and the pulsar.

In the final imaging process of PSR J0437−4715, we excluded data at short baselines of ≤20 kilo-wavelengths at 1.4 GHz to avoid some imaging errors caused by far-field bright sources. The self-calibrations were applied first with the phase only and then with both the phase and the amplitude. The calibration helped to reduce the image noise level by a factor of about four at 5 GHz. In the residual map of 1.4 GHz, the calibration also allowed us to remove some significant noise peaks (up to 19 mJy beam^{-1}).

[2] http://www.aips.nrao.edu/cook.html

2.2 New VLBI experiment at 2.3 GHz

We performed in-beam phase-referencing VLBI observations of the two candidate sources at 2.3 GHz with the Australia LBA and the Chinese Kunming 40-m radio telescope (Hao, Wang & Yang 2010) on 2015 November 18. This was the first time that the Kunming telescope had carried out an astronomical VLBI experiment together with the VLBI network of the Southern Hemisphere. The LBA participating stations included the phased-up array of the ATCA, the Parkes 64-m radio telescope, the Hobart 26-m radio telescope and the Ceduna 30-m radio telescope.

The VLBI observations lasted about six hours. The synthesized beam of the ATCA had a full width at half-maximum (FWHM) of 13.3 × 4.8 arcsec^2, which is quite narrow and insufficient to encompass PSR J0437−4715 and sources R1 and R2 simultaneously. In view of this limitation, we provided a separate schedule for the ATCA correlator to cycle its correlation phase centre among the three sources, with an interval of two minutes. The remaining telescopes have quite wide beams and thus observed all three sources with the same pointing centre. The observations had dual polarization and an observation bandwidth of 32 MHz per polarization.

The data were correlated in three passes with the Distributed FX correlator (DiFX: Deller et al. 2007). A pulsar gate, using the publicly available ephemeris for PSR J0437−4715, was used for the pass at the pulsar position. The correlator output data had 1-s integration time per data point, four sub-bands per polarization and 32 frequency points per sub-band.

The *a priori* amplitude calibration was performed in three steps. Using the attached auto-correlation data, the cross-correlation amplitude was properly scaled and corrected. According to the nominal values of system equivalent flux density provided by each station, the amplitude gain solutions were derived and applied.

Because PSR J0437−4715 is a perfect point source for both the ATCA and the VLBI network, we also used it as a flux density calibrator to improve the VLBI amplitude calibration. As an independent array, the ATCA has also provided simultaneous interferometric data. We reduced the zoom-in band data (64-MHz bandwidth) separately in MIRIAD to measure the total flux density of PSR J0437−4715. The correlation amplitude of the ATCA data was already calibrated properly through dedicated calibrator observations, so only self-calibration was performed for the ATCA data.

For the LBA data sets, delay and phase calibration were performed by running fringe-fitting on PSR J0437−4715 data with a solution interval of 1 min. In our bandpass calibration, only phase solutions were solved and applied. After these calibrations, the final solution tables were copied from the pulsar data set to the other two weak-source data sets. Because different data sets had different source ID for the same source, before we applied the solution tables we used the AIPS task TABED to adjust the source ID in the calibration table to the appropriate value as determined in the source table.

When we imaged the two faint VLA sources, we removed data on the baseline between the ATCA and the Parkes telescope, because the shortest baseline had some significantly unwanted flux originating from the nearby PSR J0437−4715 and caused some stripes in the dirty image. In future VLBI observations, the most sensitive baseline may be saved by correlating only the pulse-off data. Moreover, we removed a certain amount of ATCA data when the ATCA digital beam was off-source for each data set. With natural weighting, we achieved an image sensitivity of $1\sigma = 0.09$ mJy beam^{-1} in the final CLEAN images.

Table 3. The positions of PSR J0437−4715 and sources R1 and R2 measured by the VLBI observations on 2015 November 18.

Source	RA	Dec.	1σ (mas)
J0437−4715	$04^h37^m15^s.98936$	$-47°15'09''.6696$	0.7
R1	$04^h37^m16^s.20943$	$-47°14'56''.5046$	0.9
R2	$04^h37^m17^s.77577$	$-47°14'28''.2398$	0.9

The VLBI positions of the three sources are reported in Table 3. We measured their positions with respect to PSR J0437−4715. The position of PSR J0437−4715 was calculated from the LBA astrometric model presented by Deller et al. (2008) and was used as the correlation phase centre. The formal position error is 1σ ∼0.6 mas for sources R1 and R2. The absolute position determination of R1 and R2 is currently limited by the uncertainty in the position of PSR J0437−4715. We measured the offset of these two sources from the assumed position of PSR J0437−4715, so that any error in the latter's position is transferred. The absolute position uncertainty was obtained using differential astrometry to a single calibrator, as was the case with the earlier observations of PSR J0437−4715 (Deller et al. 2008); it is difficult to quantify and is more strongly affected by residual calibration errors than time-dependent effects such as parallax and proper motion. We re-processed the data presented in Deller et al. (2008) along with several unpublished epochs, making use of updated station positions for the LBA, and found a reference position for PSR J0437−4715 that differs by 0.7 mas from that presented in Deller et al. (2008), as well as a revised proper motion that is more consistent with the timing results of Reardon et al. (2016), differing by less than 2σ in each coordinate. The parallax value is not significantly altered. Because our ultimate goal of measuring the parallax and proper motion of PSR J0437−4715 precisely relies only on differential and not absolute positions, the absolute position uncertainty is not a main concern in this research; we assume here an uncertainty of 0.7 mas and add this in quadrature to the statistical position errors. In our future astrometric observations, we will include some phase-referenced scans from PSR J0437−4715 to J0439−4522, which has a well-determined position with an uncertainty of 0.1 mas in the International Celestial Reference Frame (ICRF), to measure the absolute position of PSR J0437−4715.

2.3 Multi-epoch ATCA observations at 8.4 GHz

PSR J0437−4715 was observed with the ATCA at 8.4 GHz for a total of seven epochs and the data are available in the Australia Telescope Online Archive. During these 8.4-GHz observations, the ATCA worked mainly as a phased-up array to participate in the LBA astrometric observations of PSR J0437−4715 (Deller et al. 2008). To search for possible flux density variability in sources R1 and R2, we also reduced these additional ATCA data to measure their total flux densities. The quite long on-source time allowed us to achieve an image sensitivity of 0.1–0.2 mJy beam^{-1} and successfully detected sources R1 and R2 in six epochs. Because of quite rapid phase variation, likely due to an instrumental issue, we failed to achieve a proper phase calibration in one epoch (V190N). In the subsequent analysis, the epoch was excluded.

In the data reduction, we used J0439−4522 as the secondary calibrator to run the self-calibration and applied its solutions to PSR J0437−4715. When the ATCA primary flux density calibrator PKS 1934 − 638 was observed, we measured the flux densities of these three sources directly. Amongst the three accurate flux-density measurements, PSR J0437−4715 has a mean flux density of 4.01 ± 0.15 mJy and a variability index of 0.08. The low variability is as expected, because the interstellar scintillation is much weaker at higher observation frequencies (e.g. Dai et al. 2015). Because PSR J0437−4715 is relatively faint at 8.4 GHz, neither the phase nor the amplitude calibrations were applicable. When PKS 1934 − 638 was not observed in the remaining three epochs (V190E, V190G and V190M), we took PSR J0437−4715 as the primary flux density calibrator and then measured the flux densities of sources R1 and R2. When the zoom-in band data (64-MHz bandwidth) were not available in the experiment V190M, we reduced the wide-band data (512-MHz bandwidth).

3 DETECTIONS OF TWO RADIO SOURCES

The VLA total intensity image at 5 GHz is shown in the middle panel of Fig. 1. Compared with PSR J0437−4715, sources R1 and R2 are quite faint. After modelling PSR J0437−4715 with a point-source model and applying self-calibration, the two faint sources are clearly visible features in the residual map. We obtained a signal-to-noise ratio (SNR) of 29 for R1 and 36 for R2 in the final image with natural weighting. The angular distance to PSR J0437−4715 is 13 arcsec for R1 and 45 arcsec for R2. Both sources are in a north-east direction and have a difference of ∼6 deg in their position angles. At the lower frequency of 1.4 GHz, both sources are fainter and source R1 is slightly brighter than source R2.

The VLBI images of sources R1 and R2 at 2.3 GHz are displayed in the left and right panels of Fig. 1. Note that the shortest baseline between the ATCA and the Parkes telescope was excluded to minimize the unwanted signal from PSR J0437−4715. This helps to improve the image sensitivity by a factor of about 2. In the final CLEAN images, we obtained an image noise level of 0.09 mJy beam^{-1} with natural weighting. The image SNRs are 8.6 for source R1 and 6.8 for source R2.

We consider R1 and R2 as real radio sources as opposed to artefacts from instrumental noise for several reasons. Both sources are the brightest peaks with SNR ≥6 in the VLBI dirty maps that have a size wide enough to cover the 5σ error circle of the VLA positions (5$\sigma \lesssim$ 0.5 arcsec). The image noise patterns surrounding the two peaks resemble the synthesized beam and show some negative peaks, which are located at the positions of negative side lobes and include the deepest one. After deconvolution of the two sources, the remaining noise peaks have SNR ≤4.6 in the residual maps. With respect to the VLA positions (our image origins), the VLBI source R1 lies at an offset of 112.7 mas and R2 at an offset of 88.9 mas, both within the 2σ error circle. Their VLBI total flux densities are also consistent with the upper limit (3$\sigma \leq$ 1.2 mJy) of our simultaneous ATCA observations at 2.3 GHz. At a flux-density level of ≥0.5 mJy, Herrera Ruiz et al. (2017) reports that faint VLA sources retain a detection fraction of ≥50 per cent at mas resolutions. Therefore, from a statistical viewpoint, it is not surprising for us to detect both in the VLBI images.

The VLBI images have a resolution 269 times higher than the VLA image. Both sources are still unresolved. Because of their compact morphology, a simple point-source model was used in measuring their total flux densities and positions. The VLA images observed simultaneously at 1.4 and 5 GHz show that the flux densities of both sources increase at higher frequencies; the inferred slightly inverted spectra are consistent with their compact appearance. The VLBI flux-density measurements of the two sources are roughly consistent with the extrapolation of the two VLA measurements from 19 yr earlier.

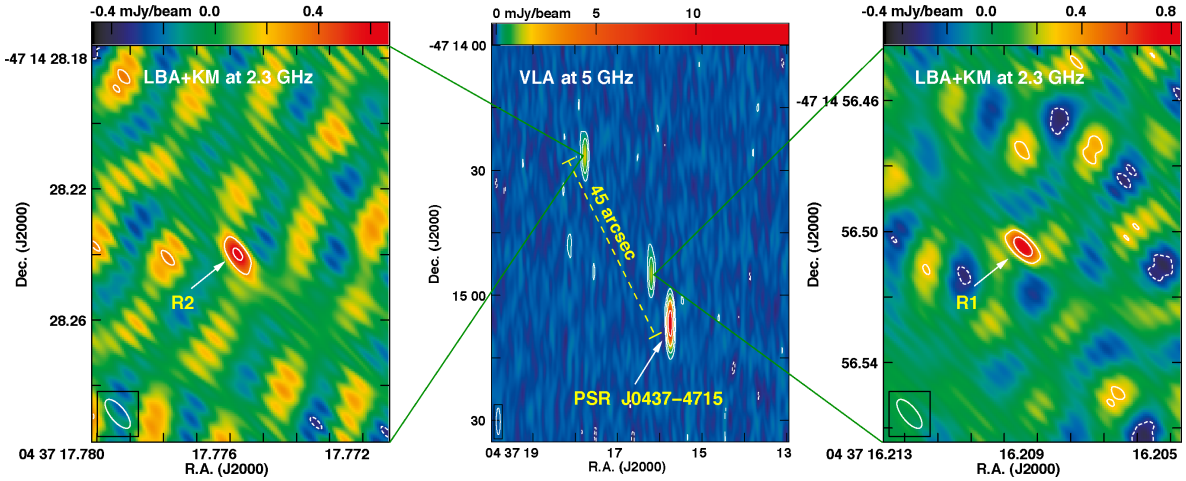

Figure 1. Radio detection of two compact radio sources (R1 and R2) with separations of 13 and 45 arcsec from the most bright and nearest millisecond pulsar PSR J0437−4715. Left: LBA+KM detection of source R2 at 2.3 GHz. Middle: Wide-field VLA 5-GHz image of the three sources. Right: LBA+KM detection of source R1. Contours start from 3σ and increase by factors of $-1, 1, 4, 8, ...$ in the VLA map and $-1, 1, 2$ in the LBA+KM map. The related image parameters are listed in Table 1.

We also fitted a circular Gaussian model to the VLBI data to derive an upper limit for their angular sizes, $\theta_{\rm size}$. We estimated $\theta_{\rm size} \leq 2.2$ mas for R1 and $\theta_{\rm size} \leq 4.0$ mas for R2. With the upper limits of $\theta_{\rm size}$, the lower limits of brightness temperature $T_{\rm b}$ in K can be estimated according to the following equation (e.g. Condon et al. 1982):

$$T_{\rm b} = 1.22 \times 10^9 \frac{S_{\rm tot}}{\nu_{\rm obs}^2 \theta_{\rm size}^2}(1+z), \quad (1)$$

where $S_{\rm tot}$ is the total flux density in mJy, $\nu_{\rm obs}$ is the observation frequency in GHz, $\theta_{\rm size}$ is the FWHM of the circular Gaussian model in mas and z is redshift. At $z = 0$, our estimation gives $T_{\rm b} \geq 4 \times 10^7$ K for R1 and $T_{\rm b} \geq 1 \times 10^7$ K for R2.

The left panel of Fig. 2 displays the total intensity image of the PSR J0437−4715 field observed by the ATCA in the first 8.4-GHz epoch. With natural weighting, the ATCA images have an image sensitivity of 0.1–0.2 mJy beam^{-1}. At the VLA positions, both sources are the brightest features, with SNRs of 4–10 in the ATCA residual maps after the deconvolution of PSR J0437−4715. The 8.4 GHz light curves of sources R1 and R2 are plotted in the right panel of Fig. 2. Compared with the average flux density, i.e. the blue line for R1 and the red line for R2, no significant deviation is detected over about 4 yr. Together with the agreement between the VLA and the VLBI results, both sources have a relatively stable flux density with a variability index of $\leq$0.15 on time-scales of months to years.

The multi-frequency flux-density measurements are also displayed in Fig. 3. Assuming that they had a relatively stable luminosity over 19 yr and a compact source structure, we can estimate their spectral indices (α, such that $S_\nu \propto \nu^\alpha$). Sources R1 and R2 have quite flat spectra ($\alpha = 0.2 \pm 0.2$ and $\alpha = 0.4 \pm 0.4$, respectively). PSR J0437−4715 has quite a steep spectrum ($\alpha = -2.0 \pm 0.1$).

4 DISCUSSION

4.1 Identifications: compact radio cores in AGNs

The most reasonable identification of sources R1 and R2 is that they are compact radio cores, i.e. stationary jet bases, in extragalactic active galactic nuclei (AGNs). This identification can naturally explain their high brightness temperatures, compact morphologies, flat radio spectra and relatively stable luminosities over 19 yr. Their brightness temperatures are clearly higher than the typical value of $\leq 10^6$ K observed in thermal emission sources, so all thermal emission origins can be firmly excluded. Currently, either jets powered by compact objects or shocks formed in certain astrophysical environments produce relativistic electrons and thus non-thermal synchrotron radio emission. Compared with the shock scenario, the AGN core scenario can naturally explain the point-like morphology and flat spectra of R1 and R2, as cores would generally have a partially self-absorbed spectrum with $\alpha \sim 0$. Moreover, shocks are usually associated with non-continuous injection of relativistic electrons and have relatively shorter lives and greater variability, whilst both sources have relatively low variability indices ($\sim$15 per cent) in the multi-epoch radio observations.

Sources R1 and R2 cannot be Galactic objects with significantly pulsed radio emission, e.g. pulsars. PSR J0437−4715 has been observed by the Parkes radio telescope for about 20 yr (Reardon et al. 2016). Because both sources are also in the same telescope beam, it is unlikely that long-term timing observations have missed any pulsed emission. Furthermore, they do not have the very steep radio spectra observed in most pulsars.

It is also quite difficult to identity sources R1 and R2 as radio jets powered by stellar-mass compact objects in the Milky Way, such as white dwarfs, neutron stars and stellar black holes in X-ray binaries. These compact objects usually have luminosities that vary significantly from radio to X-ray bands. We found no X-ray counterparts at the two locations in the image presented by Zavlin et al. (2002) with 18.9-ks High Resolution Camera observations of the *Chandra X-ray Observatory*. *XMM-Newton* MOS1 and MOS2 mosaic images of the field around PSR J0437−4715 in the 0.1–10 keV band, reported by Bogdanov (2013), also show no counterparts.

Sources R1 and R2 have no infrared and optical counterparts. This is not an unusual result, since the optical counterparts for about two-thirds of radio sources are still missing (Kimball & Ivezić 2008). Neither source was found in the all-sky data release of the *Wide-field Infrared Survey Explorer* (*WISE*) on 2012 March 14, with 5σ flux density upper limits at 3.4, 4.6, 12 and 22 μm of 0.08, 0.11, 1 and 6 mJy, respectively. We searched for their optical counterparts in the high-sensitivity image of PSR J0437−4715 observed by the

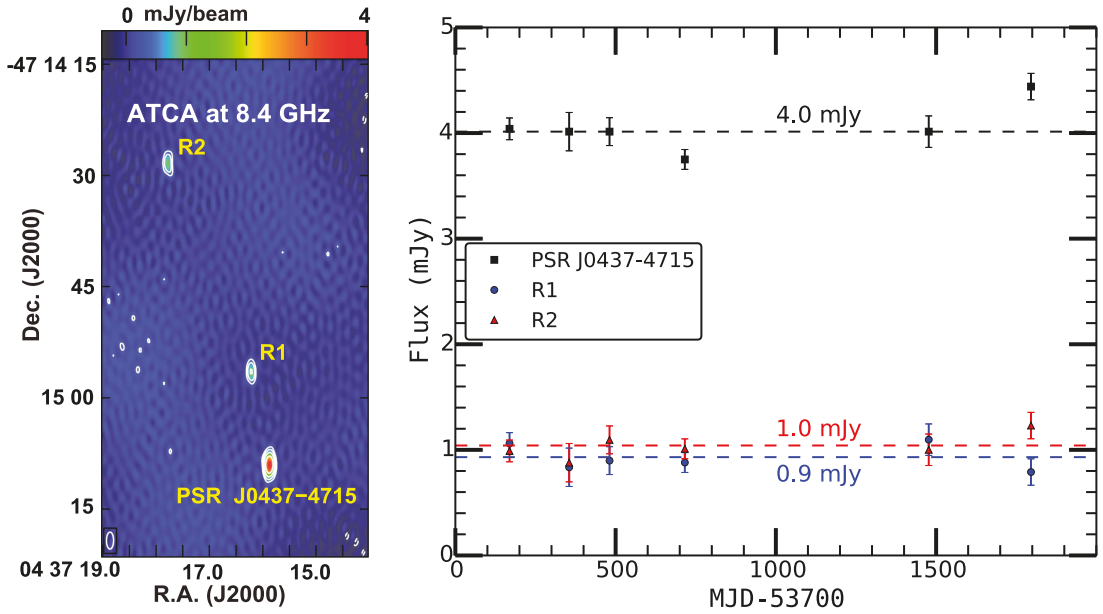

Figure 2. The radio map and light curves of PSR J0437−4715 (black) and sources R1 (blue) and R2 (red) observed by the ATCA at 8.4 GHz. In the map observed on 2006 May 13, the contours start from 3σ and increase by a factors of −1, 1, 2, 4, ... The image parameters are listed in Table 1. The flux-density measurements are reported in Table 2.

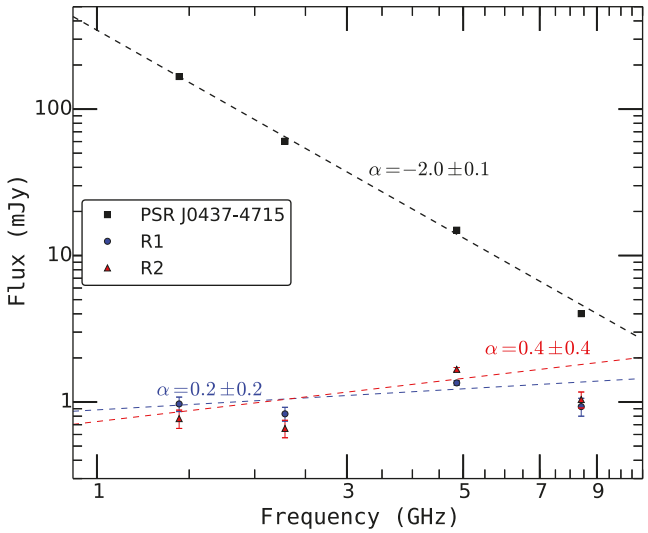

Figure 3. The radio spectra of sources R1 and R2 observed by the VLA at 1.4 and 5 GHz, the LBA+KM at 2.3 GHz and the ATCA at 8.4 GHz. The related flux measurements are summarized in Table 2.

Hubble Space Telescope with the Wide-Field Planetary Camera 2 and the F814W filter (roughly *I* band) on 1996 May 19. We find an upper limit of $m_{\rm I} = 22$ for the optical counterparts of R1 and R2, in comparison with the apparent magnitude of PSR J0437−4715 ($m_{\rm F814W} = 19.42$: Durant et al. 2012).

It is quite difficult to find a radio star even in a dedicated survey. Kimball et al. (2009) searched for candidate radio stars by comparing the survey of Faint Images of the Radio Sky at Twenty centimetre (FIRST: Becker, White & Helfand 1995) and the Sloan Digital Sky Survey (SDSS). They reported that, for the million stars in the magnitude range $15 < m_{\rm i} < 19.2$, only ≤1.2 radio stars are detected with a flux $S_{1.4} \geq 1.25$ mJy. Considering that the fraction of radio stars with flux densities above the FIRST limit declines at fainter optical magnitude, the random probability of an object being a radio star is extremely small, $\lesssim 1 \times 10^{-6}$, for R1 or R2.

Sources R1 and R2, interpreted as VLBI-detected radio cores, are likely hosted in early-type or bulge-dominated galaxies, according to the statistical study of the faint sky by Herrera Ruiz et al. (2017). VLBI is a powerful tool for revealing AGNs in some early-type galaxies without clear signs of nuclear activity in the optical and infrared bands (e.g. Park et al. 2017). Moreover, sources R1 and R2 likely belong to a group of infrared-faint radio sources (IFRS), which has a radio-to-infrared flux density ratio of the order of 100 or above (Norris et al. 2006; Maini et al. 2016).

4.2 Toward ≤10 μas VLBI astrometry

Since sources R1 and R2 are most likely compact cores in AGNs, they can be used as in-beam phase-referencing sources to perform extremely high-precision astrometry on PSR J0437−4715. They are at least 150 times closer to the pulsar than the calibrator used by Deller et al. (2008). Amongst known in-beam phase referencing observations of pulsars (e.g. Deller et al. 2013; Kirsten et al. 2015), they are the closest reference sources. It is also the first time of having multiple reference sources each with a separation of less than 1 arcmin. While previous studies have rarely sought such faint reference sources (we can make use of fainter sources, since PSR J0437−4715 itself is bright enough to provide the calibration solutions), the presence of not one but two background sources so near a target is fortuitous. The VLA survey with an angular resolution of ∼5 arcsec (FIRST: White et al. 1997) shows that the density of sources brighter than ∼1 mJy at 1.4 GHz is about 90 per square deg or one per 40 arcmin^2. A simplistic calculation gives a ∼5 per cent chance of getting one background source and just a ∼0.25 per cent chance of finding two, in a randomly selected area of 1 arcmin^2. The chance that both are compact on mas scales is even lower again. However, as shown above, we have convincing evidence that both sources are real and extragalactic in nature.

Differential VLBI astrometry on PSR J0437−4715 with respect to the two extremely nearby sources will enable us to minimize potential systematic errors, caused by the phase variations arising from propagation through the ionosphere and the troposphere, to a negligible level. Because the propagation-related components dominated the error budget, the earlier astrometric accuracy on PSR J0437−4715 is limited to 54 μas (Deller et al. 2008). The systematic errors have a tight correlation with the separation between the calibrator and the target, ∼1–2 μas per arcmin (Chatterjee et al. 2004; Deller et al. 2013; Kirsten et al. 2015). According to this empirical dependence, systematic errors will not limit the astrometric accuracy until well below ∼10 μas, which is the current best achieved result (e.g. Deller et al. 2013; Reid & Honma 2014; Yang et al. 2016). At this level, calibrator stability, rather than differential propagation errors, becomes dominant.

The two faint sources are likely extremely stable reference points. As radio cores in extragalactic AGNs, they are the most stationary parts of jet structures in the stable accretion state. There is no evidence of a major radio outburst over 19 yr of past observations. Compared with bright radio sources, faint sources may have much more stable radio cores, since they have either a much weaker Doppler beaming factor, a relatively higher redshift or an intrinsically low accretion rate. With multi-epoch European VLBI Network (EVN) in-beam phase-referencing observations at 5 GHz spanning three years, Yang et al. (2016) revealed that the radio core in a sub-mJy source has a positional stability of ≤13 μas per epoch, at least about one order of magnitude better than that of a bright source. Thus, it is quite promising for us to reach an accuracy of ≤10 μas before the core stability begins to dominate the error budget. The presence of the second in-beam calibrator provides a unique opportunity to constrain directly the potential contribution of the positional stability of the two radio cores to the astrometric accuracy. The advantages of multiple in-beam reference sources include calibration of time-varying phase errors on much shorter time-scales and higher resulting on-source durations for each source, providing better SNRs, compared with multiple reference-source observations requiring antenna slewing to cross-check the positional stability across epochs (e.g. Campbell et al. 1996) or solve for a two-dimensional propagation-induced phase-variation screen (e.g. Rioja et al. 2017). Over the next two years, we will make four astrometric observations of PSR J0437−4715 with a more sensitive VLBI network including the new Chinese Tianma 65-m radio telescope (An, Sohn & Imai 2018), which will enable us to test these predictions directly.

The new VLBI astrometry on PSR J0437−4715 can be performed at an observation frequency of ≲6.7 GHz. The small angular separations between the three sources permit the inclusion of the largest radio telescope in the Southern Hemisphere, the Tidbinbilla 70-m radio telescope, to observe them within the FWHM of a single antenna beam at a frequency up to 22 GHz. However, PSR J0437−4715 has quite a steep spectrum, $\propto \nu_{\rm obs}^{-2.0}$. To calibrate out the residual phase errors via fringe-fitting and to self-calibrate on the pulsar data with a typical baseline sensitivity limit, 1σ ∼2 mJy for two 25-m dishes, it is necessary to have a correlation amplitude of ≳10 mJy. Considering the spectral index of the pulsar, it is better to run the in-beam phase-referencing VLBI observations at a frequency of ≲6.7 GHz. By applying gating during the correlation, the SNR of the pulsar's fringes can be improved further by a factor between three from our 2.3-GHz observations and seven from the earlier 8.4-GHz observations (Deller et al. 2008). Moreover, both sources R1 and R2 will have slightly higher correlation amplitudes, because of their partially optically thick spectra at ≲6.7 GHz.

Currently, the parallax accuracy of PSR J0437−4715 can be improved by a factor of at least two with in-beam phase-referencing observations. The final VLBI image with natural weighting will have a beam size of ∼1 mas at 6.7 GHz with the currently available VLBI capabilities. With the available bandwidth of the LBA (i.e. 64 MHz), an on-source time of 300 min and all these telescopes, one can obtain a practical image sensitivity of 1σ ∼0.05 mJy beam^{-1}. Both sources R1 and R2 have a flux density of ∼1 mJy at 6.7 GHz. Thus, the VLBI images will have a SNR of 20 and a statistical astrometric accuracy of $\theta_{\rm b}/(2{\rm SNR}) \sim 25$ μas for each source. Even with only three-epoch VLBI observations, a parallax accuracy of ≲25 μas is also achievable. In the future, the parallax accuracy of PSR J0437−4715 can be continuously enhanced towards an extremely high level, ≤10 μas, with wide-band VLBI backends (e.g. Digital Base-Band Converters 3: Tuccari et al. 2014) and more VLBI stations: the Warkworth 30-m radio telescope (Petrov et al. 2015; Woodburn et al. 2015), the Nkutunse 32-m radio telescope at Kuntunse (e.g. Duah Asabere et al. 2014) and the SKA-Mid (Paragi et al. 2015).

The finding of the two sources will lead to not only a more accurate D_π for PSR J0437−4715 but also a more stringent constraint on $\dot{G}$ in the near future. The relationship between D_π and $\dot{G}$ can be simply written as (e.g. Deller et al. 2008)

$$\frac{\dot{G}}{G} = -\frac{\mu^2}{2c}(D_{\rm k} - D_\pi), \tag{2}$$

where c is the light speed and μ is the proper motion. Compared with the VLBI distance of D_π, the pulsar timing distance of $D_{\rm k}$ in equation (2) includes some excess contributions from changes intrinsic to the pulsar system, e.g. $\dot{G}$, and the differential acceleration of the Solar system and the pulsar system. Currently, μ has been measured with quite high fractional accuracy (2×10^{-5}: Reardon et al. 2016). D_π has a fractional accuracy of 0.83 per cent (Deller et al. 2008), about five times worse than the latest measurement of $D_{\rm k}$ (0.16 per cent: Reardon et al. 2016). Improvements to D_π will therefore have a direct and marked effect on the constraint on $\dot{G}/G$. Since the accuracy of $D_{\rm k}$ will rapidly improve further as the uncertainty in the observed orbital period derivative decreases with ongoing timing observations, a future comparison in which both $D_{\rm k}$ and D_π are measured to better than one part in 1000 is foreseeable, which would lead to an order-of-magnitude improvement in the uncertainty of $\dot{G}/G$.

5 CONCLUSIONS

To achieve a VLBI parallax distance with sub-pc accuracy for PSR J0437−4715, the nearest and brightest radio millisecond pulsar, via in-beam phase-referencing observations, we searched for compact radio sources near the pulsar. Within a circle of 1-arcmin radius, we detected two mJy radio sources using publicly available VLA and ATCA data. We also carried out VLBI observations of the two sources with the LBA plus the Kunming radio telescope at 2.3 GHz. Their VLBI images show that each has a compact structure and a brightness temperature of $\geq 10^7$ K. They have a flat spectrum and a relatively stable flux density over 19 yr. In the existing deep optical and X-ray images of PSR J0437−4715, we found no counterparts. Combining all these results, we argue that they are most likely compact radio cores in AGNs rather than Galactic radio stars. The existence of these two extremely nearby radio sources makes it quite promising to achieve a VLBI distance measurement at a sub-pc accuracy with the current VLBI network configuration and at a sub-light-year accuracy when more stations and wider bandwidth are

available. These continuous improvements will also lead directly to a more stringent constraint on the time stability of Newton's gravitational constant *G*.

ACKNOWLEDGEMENTS

This work was partly supported by SKA pre-construction funding from the Ministry of Science and Technology of China (2016YFE0100300) and the Chinese Academy of Sciences (CAS). TA is thankful for the grant supported by the Youth Innovation Promotion Association of CAS and FAST Fellowship, which is supported by the Centre for Astronomical Mega-Science, CAS. We thank Chris Phillips (the Australia Telescope National Facility), Zhiqiang Shen (Shanghai Astrnomical Observatory) and Min Wang (Yunnan Astronomical Observatories) for scheduling their telescope time and the station operators and engineers for supporting the joint VLBI experiment. JY thanks J. Quick, L.I. Gurvits and G. Hobbs for helpful discussion. The Australia Telescope Compact Array, Parkes radio telescope, Mopra radio telescope and Long Baseline Array are part of the Australia Telescope National Facility, which is funded by the Australian Government for operation as a National Facility managed by CSIRO. This work made use of the Swinburne University of Technology software correlator, developed as part of the Australian Major National Research Facilities Programme. This article includes archived data obtained through the Australia Telescope Online Archive (http://atoa.atnf.csiro.au). The National Radio Astronomy Observatory is a facility of the National Science Foundation operated under cooperative agreement by Associated Universities, Inc.

REFERENCES

Alpar M. A., Cheng A. F., Ruderman M. A., Shaham J., 1982, Nature, 300, 728
An T., Sohn B.-W., Imai H., 2018, Nat. Astro., 2, 118
Becker R. H., White R. L., Helfand D. J., 1995, ApJ, 450, 559
Bogdanov S., 2013, ApJ, 762, 96
Campbell R. M., Bartel N., Shapiro I. I., Ratner M. I., Cappallo R. J., Whitney A. R., Putnam N., 1996, ApJ, 461, L95
Chatterjee S., Cordes J. M., Vlemmings W. H., Arzoumanian Z., Goss W. M., Lazio T. J., 2004, ApJ, 604, 339
Condon J. J., Condon M. A., Gisler G., Puschell J. J., 1982, ApJ, 252, 102
Dai S. et al., 2015, MNRAS, 449, 3223
Deller A. T., Tingay S. J., Bailes M., West C., 2007, PASP, 119, 318
Deller A. T., Verbiest J. P. W., Tingay S. J., Bailes M., 2008, ApJ, 685, L67
Deller A. T., Boyles J., Lorimer D. R., Kaspi V. M., McLaughlin M. A., Ransom S., Stairs I. H., Stovall K., 2013, ApJ, 770, 145
Deller A. T. et al., 2016, ApJ, 828, 8
Duah Asabere B., Gaylard M., Horellou C., Winkler H., Jarrett T., 2014, in Engelbrecht C., Karataglidis S., eds., Proceedings of SAIP2014, the 59th Annual Conference of the South African Institute of Physics. Univ. of Johannesburg, South Africa, p. 296
Durant M., Kargaltsev O., Pavlov G. G., Kowalski P. M., Posselt B., van Kerkwijk M. H., Kaplan D. L., 2012, ApJ, 746, 6
Greisen E. W., 2003, in Heck A., ed., Astrophysics and Space Science Library, Vol. 285, Information Handling in Astronomy: Historical Vistas. Kluwer, Dordrecht, p. 109
Hao L.-F., Wang M., Yang J., 2010, Res. Astron. Astrophys., 10, 805
Herrera Ruiz N. et al., 2017, A&A, 607, A132
Johnston S. et al., 1993, Nature, 361, 613
Kimball A. E., Ivezić Ž. A., 2008, AJ, 136, 684
Kimball A. E., Knapp G. R., Ivezić Ž., West A. A., Bochanski J. J., Plotkin R. M., Gordon M. S., 2009, ApJ, 701, 535
Kirsten F., Vlemmings W., Campbell R. M., Kramer M., Chatterjee S., 2015, A&A, 577, 111
Maini A., Prandoni I., Norris R. P., Spitler L. R., Mignano A., Lacy M., Morganti R., 2016, A&A, 596, A80
Manchester R. N., 2015, Int. J. Modern Phys. D, 24, 1530018
Norris R. P. et al., 2006, AJ, 132, 2409
Paragi Z. et al., 2015, Proc. Sci., Very Long Baseline Interferometry with the SKA. SISSA, Trieste, PoS(AASKA14)143
Park S., Yang J., Oonk J. B. R., Paragi Z., 2017, MNRAS, 465, 3943
Petrov L., Natusch T., Weston S., McCallum J., Ellingsen S., Gulyaev S., 2015, PASP, 127, 516
Reardon D. J. et al., 2016, MNRAS, 455, 1751
Reid M. J., Honma M., 2014, ARA&A, 52, 339
Rioja M. J., Dodson R., Orosz G., Imai H., Frey S., 2017, AJ, 153, 105
Sault R. J., Teuben P. J., Wright M. C. H., 1995, in Shaw R. A., Payne H. E., Hayes J. J. E., eds, ASP Conf. Ser. Vol. 77, Astronomical data Analysis Software and Systems IV. Astron. Soc. Pac., San Francisco, p. 433
Shannon R. M. et al., 2015, Science, 349, 1522
Shepherd M. C., Pearson T. J., Taylor G. B., 1994, BAAS, 26, 987
Tingay S. J., Jauncey D. L., King E. A., Tzioumis A. K., Lovell J. E. J., Edwards P. G., 2003, PASJ, 55, 351
Tuccari G., Walter A., Salvatore B., Casey S., Felke A., Lindqvist M., 2014, in Behrend D., Baver K. D., Armstrong K. L., eds, International VLBI Service for Geodesy and Astrometry 2014 General Meeting Proceedings: 'VGOS: The New VLBI Network'. Science Press, Beijing, China, p. 86
Verbiest J. P. W. et al., 2008, ApJ, 679, 675
White R. L., Becker R. H., Helfand D. J., Gregg M. D., 1997, ApJ, 475, 479
Woodburn L., Natusch T., Weston S., Thomasson P., Godwin M., Granet C., Gulyaev S., 2015, PASA, 32, 17
Yang J., Paragi Z., van der Horst A. J., Gurvits L. I., Campbell R. M., Giannios D., An T., Komossa S., 2016, MNRAS, 462, L66
Zavlin V. E., Pavlov G. G., Sanwal D., Manchester R. N., Trümper J., Halpern J. P., Becker W., 2002, ApJ, 569, 894

This paper has been typeset from a TEX/LATEX file prepared by the author.